ARTICLES

Competition between Adiabatic and Nonadiabatic Pathways in the Photodissociation of Vibrationally Excited Ammonia†

Andreas Bach, J. Matthew Hutchison, Robert J. Holiday, and F. Fleming Crim*

Department of Chemistry, University of Wisconsin—Madison, Madison, Wisconsin 53706

Received: November 5, 2002; In Final Form: February 12, 2003

Vibrationally mediated photodissociation combined with Doppler spectroscopy and time-of-flight detection of H-atoms provides information on the photofragmentation dynamics from selected rovibrational states of $\tilde{A}^1A_2''$-state ammonia. The competition between adiabatic dissociation forming excited-state $NH_2(^2A_1)$ + H and nonadiabatic dissociation leading to ground-state $NH_2(^2B_1)$ + H products changes drastically for dissociation from different parent levels prepared by double-resonance excitation. The H-atom speed distributions suggest that the nonadiabatic dissociation channel is the major pathway except for dissociation from the antisymmetric N−H stretching (3^1) parent level, which forms exclusively $NH_2(^2A_1)$ + H. The energy disposal depends strongly on the parent state with as little as 2% of the available energy channeled into translational energy for dissociation from the 3^1 state.

Introduction

Conical intersections are an important aspect of electronically nonadiabatic processes that include essential photochemical reactions such as light harvesting.[1] Yarkony recently reviewed the theory of conical intersections.[2] The influence of coupling between Born−Oppenheimer potential energy surfaces often results in branching between energetically allowed fragmentation pathways in the photodissociation of polyatomic molecules from excited electronic states.[3] In many respects, the first singlet excited state of ammonia is a model system for nonadiabatic photodissociation dynamics.

The $\tilde{A}^1A_2''$ state of ammonia is quasibound with a barrier in the exit channel leading to the products H + NH_2. The ground electronic state of the NH_2 product ($^2B_1$) correlates with the first excited state ($^1A_2''$) of the parent, while the first excited state ($^2A_1$) of the NH_2 product correlates with the ground state ($^1A_1'$) of ammonia. In the lower symmetry of nonplanar geometries, these states have the same symmetry and form an avoided crossing, as shown in Figure 1. At planar geometries, the difference in the symmetries of the correlated electronic states allows the potential curves for the two states to cross. Experimental studies of the photofragmentation dynamics of the $\tilde{A}$ state of ammonia[4−16] identify three different dissociation pathways, the two most important being nonadiabatic and adiabatic dissociation. The competition between these two pathways governs the branching between the ground and first electronic excited states of the NH_2 fragment in the region beyond the barrier.[5,6] Below the threshold of 48551 cm^{-1} for producing electronically excited-state $NH_2(^2A_1)$ fragments, nonadiabatic dissociation forms ground-electronic-state fragments $NH_2(^2B_1)$ + H by passage through the conical intersection. Mordaunt et al.[9,10] investigated the dissociation from selected vibrational levels of $\tilde{A}$-state ammonia and found a third, state-specific contribution to the total dissociation rate that proceedes through internal conversion to high levels of the ground state.

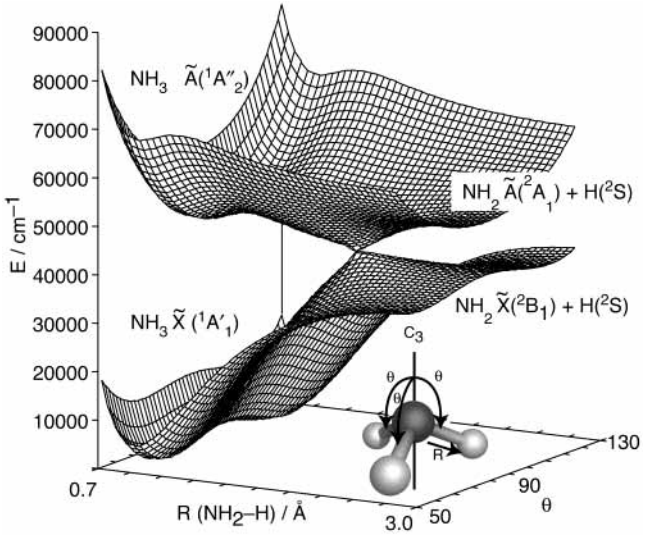

Figure 1. Cut through the $\tilde{A}$- and $\tilde{X}$-state potential energy surfaces of ammonia. The barrier to predissociation in the $\tilde{A}$ state is 2348 cm^{-1} (see ref 17)

A well-resolved progression in the excited-state out-of-plane (umbrella) bending mode dominates the $\tilde{A}-\tilde{X}$ absorption band. Each band in the progression contains transitions that have lifetime-limited widths whose dramatic variation with the vibrational quantum number reflects vibrational predissociation on the $\tilde{A}$-state potential energy surface. We recently investigated the vibronic structure of the $\tilde{A}$ state of jet-cooled ammonia using vibrationally mediated photodissociation action spectroscopy.[17]

† Part of the special issue "Charles Parmenter Festschrift."

* To whom correspondence should be addressed. E-mail: fcrim@chem.wisc.edu.

10.1021/jp027396g CCC: $25.00
Published on Web 04/26/2003

Initial vibrational excitation changes the Franck−Condon factors for the subsequent electronic transition markedly, and we assign sharp resonances to a progression in the degenerate bending mode for the first time. Our assignment reveals an accidental degeneracy of the umbrella (2^1) and bending mode (4^1) with fundamental frequencies of 892 ± 8 and 906 ± 30 cm^{-1}, respectively. We also identify broad, non-Lorentzian-shaped resonances as transitions to the symmetric (1^1) and antisymmetric N−H stretching (3^1) fundamentals.

Here we describe experiments using conventional Doppler spectroscopy combined with time-of-flight detection of H-atoms to study the photofragmentation from selected rovibrational states of Ã-state ammonia that we identify using our new excited-state assignments. In these vibrationally mediated photodissociation experiments,[18,19] infrared light excites a vibration in ammonia and a subsequent ultraviolet pulse preferentially dissociates the vibrationally excited molecules. The different Franck−Condon overlap for vibrationally excited ammonia compared to ground-state ammonia apparently results in a dissociative wave function that samples a different region of the coupled excited-state surfaces and may change the branching ratio between the $NH_2(^2A_1)$ excited-state fragments and $NH_2(^2B_1)$ ground-electronic-state fragments. Analyzing the H-atom speed distributions for dissociation from different vibronic parent states reveals highly state-specific photodissociation dynamics, particularly for states involving the stretching vibrations. Dissociation from different stretching states either promotes or inhibits the production of electronically excited NH_2 fragments, a process that hinges on the competition between adiabatic and nonadibatic dissociation pathways.

Experimental Procedure

The experimental apparatus is a modified version of one described previously.[17,20−23] A mixture of 0.1% NH_3 in helium (99.998%) at a typical backing pressure of 2000 Torr passes through a 0.4 mm orifice of a pulsed valve to form a free jet expansion that infrared vibrational excitation, ultraviolet photodissociation, and probe laser pulses intersect. Difference frequency generation in a 30 mm long $LiNbO_3$ crystal using the 1.064 μm light from an injection-seeded pulsed Nd:YAG laser and light from a dye laser provides infrared light with typical pulse energies of 0.5 to 1 mJ in a bandwidth of $\Delta\tilde{\nu}$ = 0.05 cm^{-1} at 3 μm. Frequency tripling light from a second Nd:YAG pumped dye laser provides the ultraviolet photolysis light in the 200−230 nm range. A third Nd:YAG pumped dye laser provides ultraviolet probe laser light at 243 nm for 2+1 REMPI detection of the hydrogen atoms. The infrared light arrives 20 ns before the photolysis and probe pulses at a point in the gas pulse controlled by a digital delay generator. Two different lenses (f = 150 mm and f = 350 mm, respectively) focus the counterpropagating ultraviolet and infrared laser beams into the skimmed molecular beam inside the source of a linear time-of-flight mass spectrometer, in which double-channel plates detect the resulting hydrogen ions (m/z = 1). Integrating the signal from single-laser-shot active base-line subtraction gives the increase in hydrogen ion signal due to vibrational excitation for a total of 160 laser pulses. Figure 2 shows the energetics of the vibrationally mediated photodissociation process. We prepare selected rovibrational states of Ã-state ammonia by double-resonance excitation and obtain Doppler profiles by scanning the probe laser (λ_{probe}) while detecting the total H-atom photofragment flux using 2+1 REMPI. The Doppler line shapes are independent of the relative alignment of the polarization vectors of the photolysis and infrared light, and the polarization vectors of all three pulses are parallel to the time-of-flight axis in the measurements reported here.

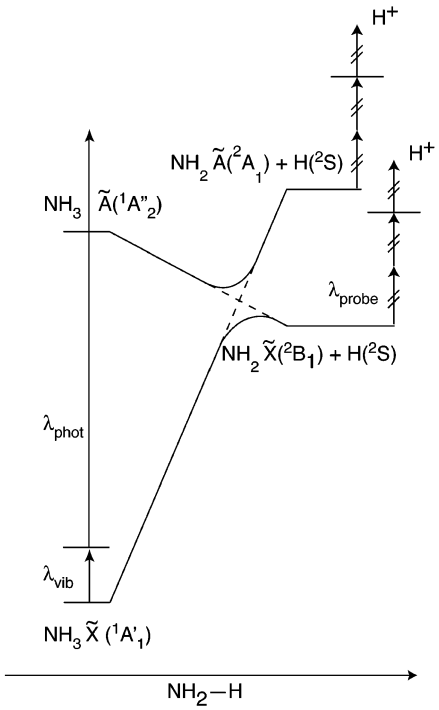

Figure 2. Schematic energy level diagram for the vibrationally mediated photodissociation of ammonia showing the relative energies of the products. The electronically excited NH_2 fragment lies 48551 cm^{-1} above ground-state NH_3, and the energy of the ground-state NH_2 fragment is 37115 cm^{-1}.

Results

We previously analyzed the vibronic structure of Ã-state ammonia to obtain the action spectra and assignments summarized in Figure 3.[17] A well-resolved progression in the excited-state umbrella mode (2^n) dominates the Ã−X̃ absorption band, which appears in the one-photon action spectrum in Figure 3a. Transitions to bending states (4^n) and antisymmetric stretching (3^1) states appear clearly in the IR−UV double-resonance experiments, along with less prominent features due to transitions to the symmetric stretch (1^1). We use vibrationally mediated photodissociation to prepare these dissociative states and analyze the Doppler profiles to extract information on the photofragmentation dynamics from these states.

We measure Doppler profiles for dissociation from rovibrational levels of Ã-state ammonia at energies marked by arrows in Figure 3. We first present and analyze the H-atom Doppler profiles for dissociation from the 0^0 state and the 2^n states and then compare the speed distributions for dissociation from these states to those for dissociation from levels in the bending (4^n) progression and from the antisymmetric (3^1) and symmetric (1^1) stretching states. The latter two states provide the most dramatic illustration of the influence of vibrational excitation on the photodissociation dynamics.

A. Dissociation from 0^0. We prepare a single rotational state in the vibrationless level of Ã-state ammonia by double-resonance excitation. A sharp transition appears in the action spectrum on the right in Figure 4, obtained following excitation to the 1_1 (J' = 1, K' = 0) intermediate state with the infrared laser. The transition is to a single lifetime-broadened resonance, the 0^0 (J = 2, K = 0) state. We tuned the photolysis laser to the center of this resonance at a total energy of 46208 cm^{-1}

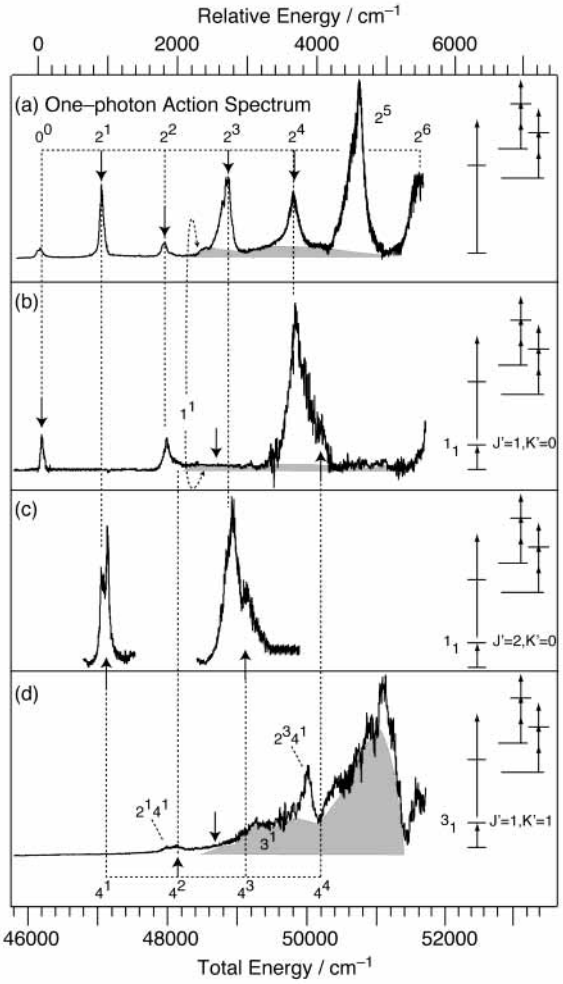

Figure 3. Overview of the action spectra of ammonia obtained from the (a) vibrationless ground state and for (b−d) different initial vibrational excitation revealing both sharp and broad features and modes that are Franck−Condon inactive in the one-photon spectrum. The assignments are discussed in detail in ref 17. The arrows show the total energies used to obtain Doppler profiles.

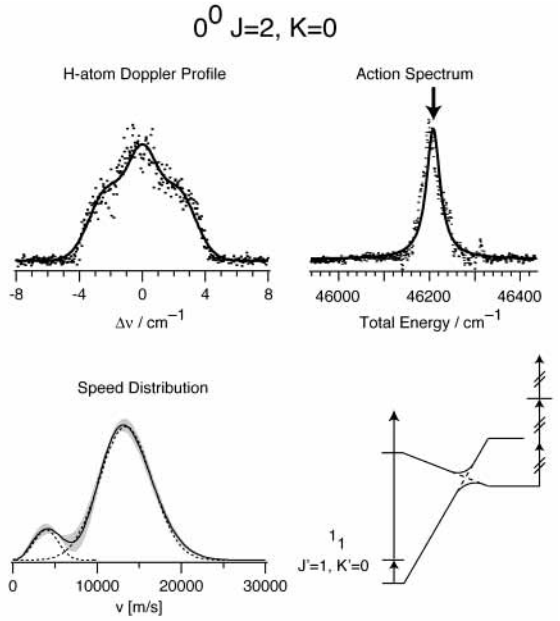

Figure 4. Doppler profiles and speed distribution obtained following double-resonance excitation to the 0^0 ($J = 2$, $K = 0$) state. The dotted lines in the speed distribution show both slow and fast components and the shaded area is the standard deviation.

and measured the Doppler profile shown on the left in Figure 4. Typically, the experimental Doppler profiles are an average of six to eight individual probe laser scans. We fit the experimental data with the procedure described by Taatjes et al.[24] and by Aoiz et al.[25] using a series of even harmonic oscillator basis functions. Five basis functions adequately represent our data. We analytically deconvolute the fitted function from the instrument response function and obtain the speed distribution $f(v)v^2$ by numerical differentiation. The resulting bimodal speed distribution also appears in Figure 4, where the shaded area indicates the standard deviation. As described in the next section, we use the two Gaussian functions plotted as dashed lines in Figure 4 to divide the speed distribution into two parts, with only 17 ± 4% coming from slow hydrogen atoms. The available excess energy $E_{\text{avail}} = h\nu - D_0(\text{H}-\text{NH}_2)$ for dissociation from the 0^0 ($J = 2$, $K = 0$) state is 9093 cm^{-1}, calculated using a bond dissociation energy $D_0(\text{H}-\text{NH}_2)$ of 37115 ± 20 cm^{-1},[1,10] and thus, the average energy released $\langle E_{\text{trans}} \rangle = 3770 \pm 150$ cm^{-1} is 41% of the available energy (Table 1). The available energy is not sufficient to form electronically excited $NH_2(^2A_1)$ photoproducts, whose threshold for production is 48551 cm^{-1}.

B. Dissociation from 2^n. The measured Doppler profiles and speed distributions for dissociation from the 2^n states ($n = 1-4$) appear in Figure 5. The well-resolved progression in the excited-state out-of-plane (umbrella) bending mode dominates the $\tilde{A}-\tilde{X}$ absorption band, which we observed in the one-photon action spectrum in Figure 3a. For odd quanta of umbrella excitation, we tuned the photolysis laser to the center of the vibronic band envelopes, exciting mainly the R(0,0) transition to access the ($J = 1$, $K = 0$) state, which contributes about 83% of the intensity. We measured Doppler profiles for dissociation from the 2^2 and 2^4 states with the photolysis laser at 47963 cm^{-1} and 49806 cm^{-1}, respectively, mainly exciting the three rotational states listed in Table 1. The distribution obtained for dissociation from the 2^2 state is clearly bimodal with maxima at 6670 m/s and 14920 m/s. The speed distribution for dissociation from the 2^1 state has a maximum at 7400 m/s while for the 2^3 and 2^4 states the maximum is at a lower velocity of ≈5300 m/s. The fraction of the available energy appearing in translation decreases from about 0.2 to 0.15 with increasing excitation of the umbrella mode, as shown in Figure 6.

C. Dissociation from 4^n. The measured Doppler profiles and speed distributions for dissociation from single rotational levels for one to four quanta of bending excitation in the $\tilde{A}$ state of ammonia appear in Figure 7. Table 1 lists the major contribution of rotational levels accessed for each vibrational state and the different intermediate states used in the double-resonance excitation scheme. The speed distribution for dissociation from the 4^4 state is clearly bimodal and similar to the distribution for dissociation from the 0^0 state. The distributions for dissociation from other states in the bending progression have maxima at 8280 m/s for 4^1, 6630 m/s for 4^2, and 9650 m/s for the 4^3 state. The average translational energy release for the hydrogen atoms for dissociation from all levels of bending excitation is smaller than from the 0^0 state, even though more energy is available, as listed in Table 1. This situation results in a much smaller fraction $\langle f_{\text{trans}} \rangle$ of the available excess energy being channeled into translational energy. The fraction is nearly constant at 20% for dissociation from different quanta of bending motion and similar to dissociation for the nearly isoenergetic 2^n umbrella states. Figure 6 compares $\langle f_{\text{trans}} \rangle$ for dissociation from different levels, including states in the bending progression

TABLE 1: Average Translational Energy Release and Its Fraction of the Available Energy for Dissociation from Selected Rovibronic States of Ammonia

state[a]	intermediate state	total energy (cm^{-1})	available energy (cm^{-1})	$\langle E_{trans} \rangle$ (cm^{-1})	$\langle f_{trans} \rangle$	fraction fast
2^1 ($J=1, K=0$)		47060	9945	1880 ± 110	0.19 ± 0.01	0.38 ± 0.06
2^2 ($J=2, K=0$) ($J=2, K=1$) ($J=1, K=1$)		47963	10848	2300 ± 90	0.21 ± 0.01	0.33 ± 0.01
2^3 ($J=1, K=0$)		48870	11755	1740 ± 160	0.15 ± 0.01	0.31 ± 0.04
2^4 ($J=2, K=0$) ($J=2, K=1$) ($J=1, K=1$)		49806	12691	1680 ± 90	0.13 ± 0.01	0.27 ± 0.04
0^0 ($J=2, K=0$)	1_1 ($J'=1, K'=0$)	46208	9093	3770 ± 150	0.41 ± 0.02	0.83 ± 0.04
1^1 ($J=2, K=0$) ($J=0, K=0$)	1_1 ($J'=1, K'=0$)	48700	11585	3490 ± 450	0.30 ± 0.04	0.75 ± 0.04
3^1 ($J=2, K=2$)	3_1 ($J'=1, K'=1$)	48700	11585	260 ± 90	0.02 ± 0.01	0.0
4^1 ($J=1, K=1$)	1_1 ($J'=2, K'=0$)	47032	9917	1710 ± 200	0.17 ± 0.02	0.56 ± 0.12
4^2 ($J=2, K=2, l=-2$)	3_1 ($J'=1, K'=1$)	48124	11009	1880 ± 380	0.17 ± 0.03	0.53 ± 0.04
4^3 ($J=3, K=1, l=2$)	1_1 ($J'=2, K'=0$)	49145	12030	2680 ± 150	0.22 ± 0.01	0.71 ± 0.02
4^4 ($J=2, K=0$)	1_1 ($J'=1, K'=0$)	49994	12879	2259 ± 280	0.17 ± 0.02	0.52 ± 0.03

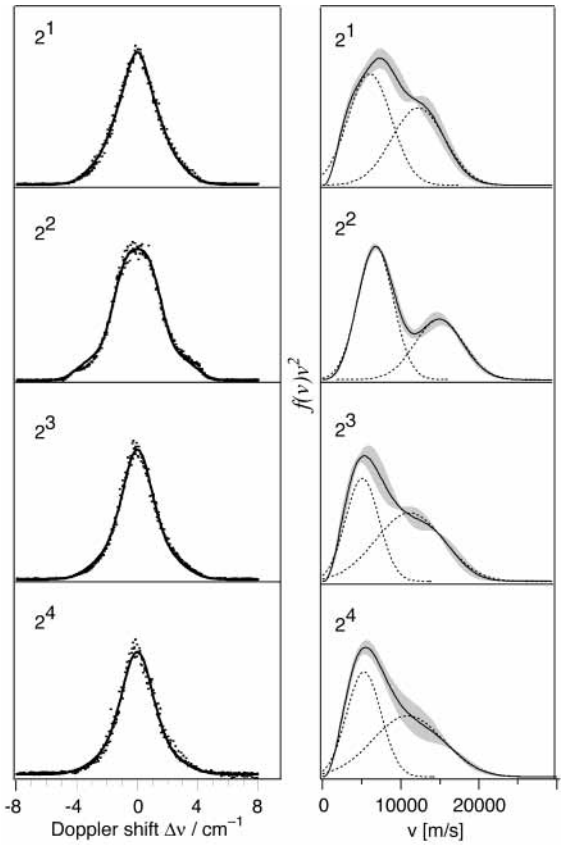

Figure 5. Doppler profiles and speed distributions for dissociation from the Ã-state umbrella fundamental and overtones accessed by one-photon excitation.

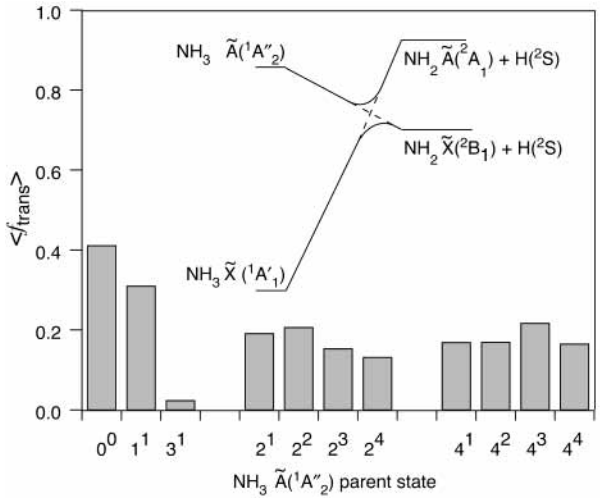

Figure 6. Average translational energy release for dissociation of selected rovibronic levels of Ã-state ammonia.

and shows that the excess energy disposal depends strongly on the initially prepared state. The low fraction of excess energy appearing in translation for dissociation from the bending states also implies that the NH_2 fragments are born with high levels of internal excitation.

D. Dissociation from 3^1 and 1^1. Both stretching states 3^1 and 1^1 couple strongly to the dissociation continuum and appear as the broad spectral transitions shown with shaded areas in Figure 3. We obtain a Doppler profile for dissociation from the symmetric stretching state of Ã-state ammonia at a total energy of 48700 cm^{-1}, marked by an arrow in Figure 3b, ≈480 cm^{-1} higher in energy than the onset of the band. For the antisymmetric stretching state, we use a different intermediate state in double-resonance excitation listed in Table 1 to prepare the 3^1 ($J=2, K=2$) state selectively at a total energy of 48700 cm^{-1}, ≈300 cm^{-1} above the onset of that band. Table 1 gives the total energy, available energy, and the selected rotational states.

Figure 8 shows the Doppler profiles and speed distributions obtained for dissociation from the symmetric and antisymmetric stretching states of Ã-state ammonia. The Doppler profile for dissociation from the antisymmetric 3^1 state has nearly a Gaussian shape and is much narrower than the profile for dissociation from 1^1. The average translational energy release for dissociation from 1^1 is 3490 ± 450 cm^{-1}, 10 times more than that for dissociation from the 3^1 state, even though the total energies are the same. The speed distributions are also very different with a bimodal distribution for 1^1 with maxima at 5520 and 13850 m/s and a single maximum corresponding to slow hydrogen atoms with speeds <5000 m/s for 3^1. Figure 6 shows that $\langle f_{trans} \rangle = 2\%$ for dissociation from 3^1 with most of the energy appearing in internal energy of the NH_2 photofragment while for dissociation from 1^1 about 30% of the available energy appears in translation.

Discussion

The state-selective photofragmentation dynamics of the first electronically excited state ($\tilde{A}^1A_2''$) of ammonia in our vibrationally mediated photodissociation experiments are consistent with previous experimental studies for dissociation from the vibrationless level and from umbrella states.[4−16] Vibrationally mediated photodissociation allows preparation of single rovibronic levels of the symmetric and antisymmetric stretching states, as well as bending parent states, for the first time. Dissociation from these states promotes or inhibits the production of electronically excited NH_2 fragments, a process that

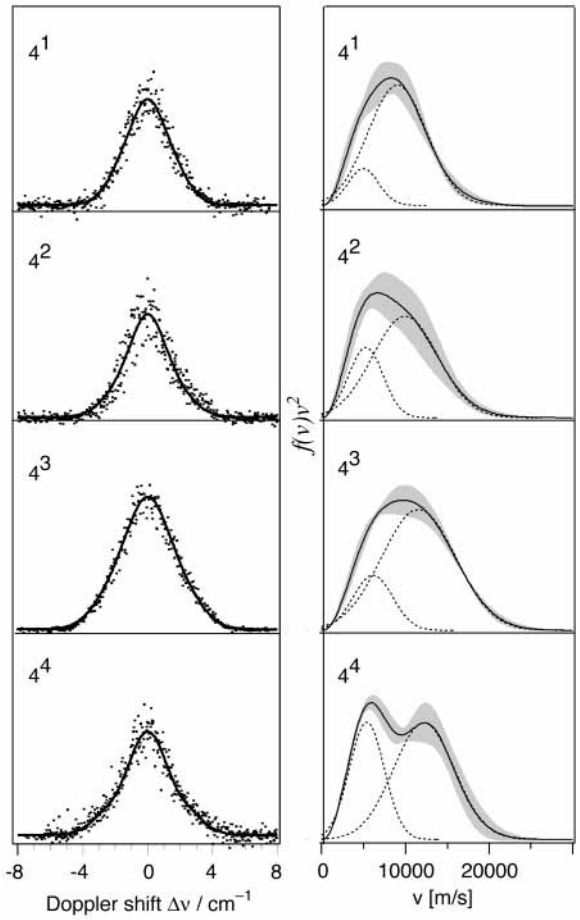

Figure 7. Doppler profiles and speed distributions for dissociation from the Ã-state bending fundamental and overtones. Single rovibronic levels are prepared by double-resonance excitation with the intermediate and final states listed in Table 1.

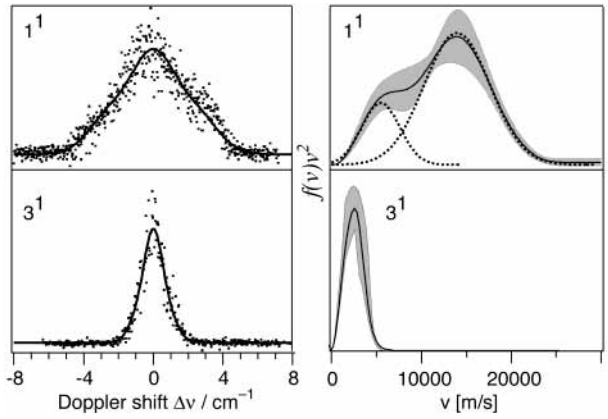

Figure 8. Doppler profiles and speed distributions for dissociation from the symmetric stretch and antisymmetric stretch of Ã-state ammonia.

involves the competition between adiabatic and nonadibatic dissociation pathways.

The three different dissociation pathways lead to very different energy deposition in the photofragments. The nonadiabatic dissociation channel forms ground-electronic-state fragments $NH_2(^2B_1)$ + H by passage through the conical intersection and mainly forms fast hydrogen atoms while both internal conversion and adiabatic dissociation result in slow hydrogen atoms. The bimodal character of the speed distributions depends strongly on the parent state. We simultaneously fitted all speed distributions with two Gaussians to calculate

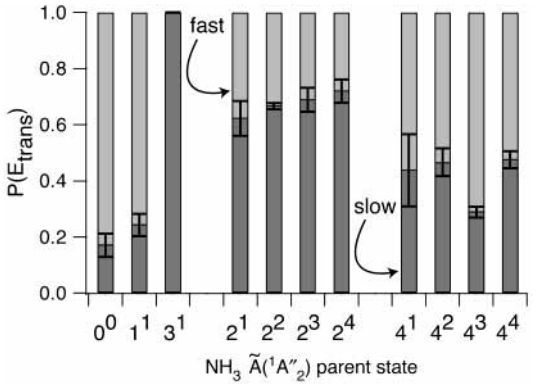

Figure 9. Fractions of slow and fast hydrogen atoms extracted form the bimodal speed distributions as a function of parent vibronic level.

the fraction of slow and fast hydrogen atoms for dissociation from the selected rovibronic states, except for the case of 3^1. The simplest model with the fewest fitting parameters that reproduces our data includes a Gaussian function centered at 6525 m/s with a fixed width (fwhm) of 3555 m/s for all slow hydrogen atoms and a Gaussian that has a width and center that scale linearly with excess energy for all fast hydrogen atoms. Fits with fewer constraints did not yield better residuals, and the fraction for the slow and fast hydrogen atoms differed by no more than 10% for different models. Figure 9 shows the average fractions for the slow and fast hydrogen atoms for five fits to the speed distributions with different constraints. The uncertainty ranges shown in Figure 9 are the standard deviation from these average fractions. To understand these observations, we briefly review the dissociation dynamics for each different dissociation pathway and discuss the state-selective change in the competition between the adiabatic and nonadiabatic pathways.

A. Internal Conversion. Mordaunt et al.[9,10] investigated the photodissociation from the 0^0 and 2^1 levels of Ã-state ammonia and its deuterated isotopomers and assigned sharp features in the kinetic energy release spectra to a population of a subset of vibronic levels in ground-state $NH_2(^2B_1)$. They also found a background continuum at low kinetic energy. This background is consistent with a statistical distribution over the vibrational and rotational degrees of freedom in the $NH_2(^2B_1)$ photofragments. The authors assigned the continuum to state-specific dissociation of the parent molecules by internal conversion to high levels of the ground state. In their picture, the statistical contribution to the kinetic energy release spectra arises from molecules that miss the conical intersection on the first pass and only make the Ã → X̃ transfer on a later encounter during NH_2-H bond compression.[4]

The contribution of slow hydrogen atoms shown in Figure 9 could, in principle, arise from internal conversion. The total fraction of slow hydrogen atoms for dissociation from 0^0 is only 0.17 ± 0.04, but it is 1.0 for dissociation from 3^1. For the progression in the umbrella mode (2^n), the fraction of slow hydrogen atoms is nearly constant at ≈0.65, while for the progression in the bend (4^n) it is only ≈0.40. The rates of internal conversion depend on the ground-state density of states and the matrix elements coupling the Ã and X̃ states. A harmonic-vibrational-state count gives a density of states in the ground electronic state at the energy of the 0^0 state of ≈40 cm^{-1}. Internal conversion must preserve nuclear permutation symmetry, and the effective background density of states is only one-sixth of the total density of states for states with A_1 and A_2 vibronic symmetry but is two-thirds for states with E vibronic symmetry.[9]

If all slow hydrogen atoms arise from internal conversion, then the fraction of slow hydrogen atoms in Figure 9 should increase with increasing energy and a corresponding increasing effective density of states. Furthermore, dissociation from states of E vibronic symmetry (3^1,4^1,4^2, and 4^3) should have a larger fraction of slow hydrogen atoms than for dissociation from states with A_1 (2^1 and 2^3) or A_2 (0^0, 1^1, 2^2, 2^4, and 4^4) vibronic symmetry. Figure 9 clearly shows that the observed trends are different and that internal conversion is only a minor dissociation pathway, in agreement with the results of Mordaunt et al.[9]

B. Nonadiabatic Dissociation Channel. Below the threshold of 48551 cm^{-1} for producing electronically excited-state $NH_2(^2A_1)$ fragments, nonadiabatic dissociation forms ground-electronic-state fragments $NH_2(^2B_1)$ + H by passage through the conical intersection. The energies of the 0^0, 2^n, and 4^n ($n < 3$) states are below this threshold. Biesner et al.[5,6] first investigated the product quantum-state distributions resulting from photodissociation of Ã-state ammonia using H-atom photofragment translational spectroscopy. Dissociation from the electronic origin yielded ground-state NH_2 photofragments mostly in their zero-point vibrational level and a nearly statistical population distribution over the energetically accessible product rotational levels with $N \sim K_a$. In the picture of Mordaunt et al.,[10] this rotational excitation arises from the substantial out-of-plane torque acting at the conical intersection to produce angular momentum in the products. This product distribution has both fast and slow hydrogen atoms, which we also observe in the speed distribution obtained for dissociation from 0^0.

In contrast, dissociation from umbrella (2^n) parent levels produces highly inverted rotational population distributions over the $N \sim K_a$ rotational states and a higher level of vibrational excitation,[5,6] resulting in a larger fraction of slow hydrogen atoms. The fraction of slow hydrogen atoms for dissociation from 2^n shown in Figure 9 is 4 times larger than that for dissociation from 0^0. This trend mainly reflects the increasing amount of rotational and vibrational excitation in the NH_2 fragment with increasing quantum number *n*, which agrees with the results of Biesner et al.[5,6]

The Doppler profiles for dissociation from 4^n appearing in Figure 7 closely resemble the profiles for dissociation from 2^n shown in Figure 5, and the fraction of excess energy appearing as product translational energy is also very similar, as shown in Figure 6. The parent bending motion correlates adiabatically with the bending motion ν_2 of the NH_2 product. Calculations by Dixon[26] predict the loss of one quantum of bending excitation and a rotational product distribution with $N \sim K_a$ for dissociation from the parent bend. Inspection of Figure 9 and Table 1 shows that, for the same quantum number *n*, dissociation from the bend (4^n) results in slightly more fast hydrogen atoms compared to dissociation from the corresponding umbrella (2^n) level. The speed distributions obtained for dissociation from all 4^n and 2^n levels have less bimodal character compared to dissociation from 0^0, and the separation into slow and fast components is not unique. The larger fraction of fast hydrogen atoms for dissociation from 4^n compared to 2^n may, however, suggest less vibrational excitation in the NH_2 photofragment for dissociation from the bend.

The speed distribution for dissociation from the symmetric stretch (1^1) appears in Figure 8 and has the same shape as the distribution for dissociation from the vibrationless level. The large fraction of fast hydrogen atoms indicates an essentially direct nonadiabatic dissociation through the conical intersection along a coordinate that conserves C_{2v} symmetry.[26] The similarity of the speed distributions suggests that the product distribution for dissociation from 1^1 is similar to 0^0 with almost no vibrational excitation in the NH_2 photofragment.

C. Adiabatic Dissociation Channel. Biesner et al.[6] found that the adiabatic dissociation channel producing electronically excited-state $NH_2(^2A_1)$ fragments opens at the energetic threshold for dissociation from the 2^n ($n > 2$) states. Loomis et al.[8] observed a bimodal $N = K_a$ rotational distribution in $\nu_2 = 0$ of the $NH_2(^2A_1)$ photofragments for dissociation from 2^6, which they suggested may result from the competition between planar and bent geometries during dissociation. The quantum yield for forming $NH_2(^2A_1)$ fragments for dissociation from 2^3 and 2^4 is only ≈ 0.1.[6] Thus, the fraction of slow hydrogen atoms shown in Figure 9 reflects the amount of highly rotationally and vibrationally excited ground-state $NH_2(^2B_1)$ photofragments with a minor contribution of internal conversion and electronically excited $NH_2(^2A_1)$ photofragments for dissociation from all states except the antisymmetric stretch.

The speed distribution for dissociation from 3^1 shown in Figure 7 has only very slow hydrogen atoms in contrast to the distributions for dissociation from all the bending, umbrella, and symmetric stretching states. The available excess energy for dissociation from the 3^1 state is 11585 cm^{-1}, just above the threshold to populate the lowest rotational states in the $NH_2(^2A_1)$ product. *The production of only slow H atoms suggests that the adiabatic pathway dominates in dissociation from the antisymmetric stretch (3^1).* In this picture, dissociation from 3^1 yields only $NH_2(^2A_1)$ photofragments while dissociation of ammonia prepared in the isoenergetic 1^1 state yields only $NH_2(^2B_1)$ photofragments. Both stretching states have planar geometries during dissociation, and a simple competition between planar and nonplanar dissociation cannot explain the highly state-selective photodissociation dynamics. Dissociation from the 1^1 level, however, is more likely to conserve C_{2v} symmetry than dissociation from the 3^1 level. Trajectories starting from the 3^1 state are more likely to bypass the deep funnel of the conical intersection in the exit channel and preferentially stay on the upper adiabatic surface leading to the $NH_2(^2A_1)$ + H products.

Conclusions

Vibrationally mediated photodissociation combined with Doppler spectroscopy and time-of-flight detection of the H-atoms provides new information on the photofragmentation dynamics from selected rovibrational states of Ã-state ammonia. Initial vibrational excitation changes the Franck−Condon factors for the subsequent electronic transition markedly and allows preparation of single rotational levels of parent bending and stretching states in addition to umbrella states and the vibrationless level.

The H-atom speed distributions show that the nonadiabatic dissociation channel is the major pathway for dissociation from all umbrella, bending and symmetric stretching states. Internal conversion plays a minor role in dissociation from all states, as the fraction of slow hydrogen atoms does not correlate with the effective density of states. We conclude that the adiabatic pathway dominates dissociation from the antisymmetric stretch (3^1) state consistent with the narrow speed distribution of slow hydrogen atoms. Dissociation from the 3^1 level is less likely to conserve C_{2v} symmetry during dissociation in contrast to the 1^1 level prepared with the same amount of excess energy. In this picture, trajectories starting from the 3^1 state are more likely to bypass the deep funnel of the conical intersection in the exit channel and preferentially stay on the upper adiabatic surface to form the $NH_2(^2A_1)$ + H products.

The energy disposal depends strongly on the parent state, with as little as 2% of the available energy channeled into H-atom translational energy for dissociation from the 3^1 state but with 20%−40% entering translation for all other vibrations of $\tilde{A}$-state ammonia. The experiments described here along with additional recent measurements using H-Rydberg-atom photofragment translational spectroscopy[27] reveal highly excited NH_2 photofragments for dissociation from the bend and umbrella states, while dissociation from the vibrationless level and the symmetric stretching parent state results in vibrationally cold NH_2. The competition between adiabatic and nonadiabatic dissociation changes drastically for different parent levels prepared with double-resonance excitation. Further theoretical studies are potentially a key complement to these experiments and will provide more insight into the photofragmentation dynamics.

Acknowledgment. We gratefully acknowledge the support of this work by the Division of Chemical Sciences of the Office of Basic Energy Sciences of the Department of Energy. A.B. thanks the Schweiz. Nationalfonds for a fellowship.

References and Notes

(1) Hu, X.; Schulten, K. *Phys. Today.* **1997**, *50*, 28.
(2) Yarkony, D. R. *J. Phys. Chem. A* **2001**, *105*, 6277.
(3) Butler, L. J. *Annu. Rev. Phys. Chem.* **1998**, *49*, 125.
(4) Ashfold, M. N. R.; Dixon, R. N.; Kono, M.; Mordaunt, D. H.; Reed, C. L. *Philos. Trans. R. Soc. London, Ser. A* **1997**, *355*, 1659.
(5) Biesner, J.; Schnieder, L.; Schmeer, J.; Ahlers, G.; Xie, X.; Welge, K. H.; Ashfold, M. N. R.; Dixon, R. N. *J. Chem. Phys.* **1988**, *88*, 3607.
(6) Biesner, J.; Schnieder, L.; Ahlers, G.; Xie, X.; Welge, K. H.; Ashfold, M. N. R.; Dixon, R. N. *J. Chem. Phys.* **1989**, *91*, 2901.
(7) Dixon, R. N.; Hancock, T. W. R. *J. Phys. Chem. A* **1997**, *101*, 7567.
(8) Loomis, R. A.; Reid, J. P.; Leone, S. R. *J. Chem. Phys.* **2000**, *112*, 658.
(9) Mordaunt, D. H.; Dixon, R. N.; Ashfold, M. N. R. *J. Chem. Phys.* **1996**, *104*, 6472.
(10) Mordaunt, D. H.; Ashfold, M. N. R.; Dixon, R. N. *J. Chem. Phys.* **1996**, *104*, 6460.
(11) Reid, J. P.; Loomis, R. A.; Leone, S. R. *J. Chem. Phys.* **2000**, *112*, 3181.
(12) Reid, J. P.; Loomis, R. A.; Leone, S. R. *Chem. Phys. Lett.* **2000**, *324*, 240.
(13) Reid, J. P.; Loomis, R. A.; Leone, S. R. *J. Phys. Chem. A* **2000**, *104*, 10139.
(14) Vaida, V.; McCarthy, M. I.; Engelking, P. C.; Rosmus, P.; Werner, H. J.; Botschwina, P. *J. Chem. Phys.* **1987**, *86*, 6669.
(15) Vrakking, M. J. J.; Ashfold, M. N. R.; Dixon, R. N.; Mills, I. M. *Philos. Trans. R. Soc. London, Ser. A* **1997**, *355*, 1674.
(16) Woodbridge, E. L.; Ashfold, M. N. R.; Leone, S. R. *J. Chem. Phys.* **1991**, *94*, 4195.
(17) Bach, A.; Hutchison, J. M.; Holiday, R. J.; Crim, F. F. *J. Chem. Phys.* **2002**, *116*, 9315.
(18) Crim, F. F. *J. Phys. Chem.* **1996**, *100*, 12725.
(19) Crim, F. F. *Annu. Rev. Phys. Chem.* **1993**, *44*, 397.
(20) Penn, S. M.; Hayden, C. C.; Muyskens, K. J. C.; Crim, F. F. *J. Chem. Phys.* **1988**, *89*, 2909.
(21) Galloway, D. B.; Glenewinkelmeyer, T.; Bartz, J. A.; Huey, L. G.; Crim, F. F. *J. Chem. Phys.* **1994**, *100*, 1946.
(22) Thorson, G. M.; Cheatum, C. M.; Coffey, M. J.; Crim, F. F. *J. Chem. Phys.* **1999**, *110*, 10843.
(23) Bach, A.; Hutchison, J. M.; Holiday, R. J.; Crim, F. F. *J. Chem. Phys.* **2002**, *116*, 4955.
(24) Taatjes, C. A.; Cline, J. I.; Leone, S. R. *J. Chem. Phys.* **1990**, *93*, 6554.
(25) Aoiz, F. J.; Brouard, M.; Enriquez, P. A.; Sayos, R. *J. Chem. Soc., Faraday Trans.* **1993**, *89*, 1427.
(26) Dixon, R. N. *Mol. Phys.* **1996**, *88*, 949.
(27) Bach, A.; Hutchison, J. M.; Holiday, R. J.; Crim, F. F. *J. Chem. Phys.* **2003**. In press.